SIMULATION OF PROTON RF CAPTURE IN THE AGS BOOSTER*

F.Z. Khiari, A.U. Luccio, W.T. Weng

Brookhaven National Laboratory
Associated Universities Inc.
Upton, New York 11973

Abstract

RF capture of the proton beam in the AGS Booster has been simulated with the longitudinal phase-space tracking code ESME. Results show that a capture in excess of 95% can be achieved with multiturn injection of a chopped beam.

Introduction

The AGS Booster[1] is a fast cycling accelerator designed to inject high intensity beams of protons and heavy ions into the AGS. It is very important to minimize the losses of these high intensity beams or, equivalently, to maximize the percentage of particles captured inside the rf bucket. Numerical simulation is the most reliable way to study this process. To this end, the computer code ESME[2] was adapted and modified to be used at BNL as a design tool. In particular, it was used to study the physics of the capture process in the AGS Booster and its dependence on machine parameters.

Beam Induced Effects

In ESME, a number of macroparticles are tracked in the longitudinal phase space. A pair of hamiltonian difference equations is solved for each macroparticle on each turn. The percentage of particles captured inside the rf bucket is calculated as a function of the specified accelerating voltage $V(t)$ and the time rate of change of the magnetic guide field $\dot{B}(t)$. The phase space coordinates used in ESME are the total energy E (MeV) and the azimuth θ ($-\pi \leq \theta \leq \pi$) measured with respect to the energy E_s and the azimuth θ_s of the synchronous particle. The equations of motion for particle i on turn number n are:

$$E_{i,n} = E_{i,n-1} + eV_n sin(h\theta_{i,n} + \psi_n) + \delta E^{sc}_{i,n}, \quad (1)$$

$$\theta_{i,n} = \theta_{i,n-1} + 2\pi(\frac{\omega_s}{\omega_{i,n}} - 1), \quad (2)$$

where e is the proton's charge, V is the rf voltage amplitude, $h \equiv \omega_{rf}/\omega_s$ is the rf harmonic number, ψ is a reference phase (usually $\psi = h\theta_s$), ω is the revolution frequency, and δE^{sc} is the energy change due to space charge, beam-wall coupling impedances and rf parasitic modes. The space charge voltage is calculated for the case of a uniform cylindrical beam of radius a centered in a round pipe of radius b. These three energy contributions are combined in ESME by expressing all of them in terms of the beam current. This beam current is Fourier analyzed and the voltage due to each beam component is calculated separately. The constant of proportionality between the beam current and the beam induced voltage is a complex impedance with frequency dependence. The total longitudinal impedance is

$$Z(\omega) = Z^{sc}(\omega) + Z^W(\omega) + Z^R(\omega), \quad (3)$$

where

$$Z^{sc}(\omega) = -j\frac{Z_0 g(\omega/\omega_{rf})}{2\beta\gamma^2}, \quad (4)$$

is the longitudinal space charge impedance, $Z^W(\omega)$ is the (broad band) wall impedance, and

$$Z^R(\omega) = \frac{R_{sh}}{1 + iQ(\omega/\omega_r - \omega_r/\omega)} \quad (5)$$

is the impedance of the rf parasitic mode. In the above formulas, $Z_0 = 377\Omega$ is the vacuum impedance, β and γ are the usual relativistic factors, $g = 1 + 2ln(b/a)$, and R_{sh}, Q and ω_r are respectively the shunt impedance, the quality factor and the resonance frequency of the rf parasitic mode. For the AGS Booster $a \approx 2.5\ cm$, $b \approx 7.5\ cm$ and with $n \equiv \omega/\omega_{rf}$, we get $Z^{sc}/n \approx -j700\ \Omega$ at injection energy (200 MeV kinetic energy) and $Z^{sc}/n \approx -j100\ \Omega$ at extraction energy (1500 MeV kinetic energy). These are large impedances and are likely to be the main cause of beam loss in the ring.
The total beam induced voltage is then

$$V^b(\theta) = \sum_n Z(n\omega_s) I_n(\theta), \quad (6)$$

where I_n is the n^{th} Fourier component of the beam current

$$I_n = eN\omega_{rf} a_n e^{i(n\theta + \theta_n)}. \quad (7)$$

N is the number of particles per bunch and a_n and θ_n are the real amplitude and phase of the n^{th} component of the Fourier spectrum of the beam current. The resulting energy change is then

$$\delta E^{sc} = \Re(eV^b) = e^2 N\omega_{rf}$$

$$\times \Re \sum_n [Z^W(n\omega_s) + Z^R(n\omega_s) - j\frac{nZ_0 g}{2\beta\gamma^2}] a_n e^{i(n\theta - \theta_n)}, \quad (8)$$

where $\Re$ denotes the real part and only the space charge term is included in the following studies.

For the numerical simulation, we generate the Fourier decomposition of the beam current by first binning the longitudinal distribution of the particles. The Fourier coefficients are then obtained by a Fast Fourier Transform of the bin occupation numbers. In our simulations we found some dependence of the capture efficiency on the number of bins for a given number of macroparticles. The choice of the number of bins is dictated by both physical and computational considerations. Obviously, too few bins give a poor representation of the particles' distribution. On the other hand too many bins give a good representation only if there are enough macroparticles. Moreover, the microwave cutoff consideration leads to an upper limit on the number of beam harmonics to be included in equation (8). The cutoff for the lowest (TE_{11}) mode of a circular pipe of radius b is

$$\lambda_c = 3.4126b. \quad (9)$$

Therefore, the maximum number of Fourier components is

$$n_c^{max} = \frac{\lambda_{rf}^{beam frame}}{\lambda_c} = \frac{\gamma\lambda_{rf}^{lab. frame}}{3.4126b}. \quad (10)$$

Similarly, the maximum number of bins that is consistent with

* Work performed under the auspices of the U.S. Department of Energy.

the microwave cutoff is

$$n_{bin}^{max} = 2n_c^{max} = \frac{2\gamma\lambda_{rf}}{3.4126b}. \quad (11)$$

This maximum number of bins corresponds to a minimum bin length, or equivalently a minimum interaction length between adjacent bins, below which the fields generated by one bin travel freely along the beam pipe at a speed different from that of the bunch and therefore do not contribute to space charge effects. For the AGS Booster $\gamma \approx 1.2$, and $\lambda_{rf} \approx 120\ m$ for the early part of the cycle. Thus

$$n_{bin}^{max} \approx 1000 \quad (12)$$

This number is rather large in our application, so the limit on the number of bins is generally dictated by the number of particles in the simulation and ultimately by the computing time.

Simulation of Proton rf Capture

Multiturn injection

We did three series of studies. In the first study, we established that rf capture with multiturn injection is more efficient than with single turn injection. This difference can be attributed to the fact that space charge is incrementally built up for multiturn injection. Its effect is small at the beginning and the total effect is felt only after injection is finished. In the case of single turn injection, however, the total space charge force is felt at the beginning. This effect is particularly strong after a quarter period of synchrotron oscillations when the azimuthal distribution of the particles in the bunch is very peaked around the synchronous particle.

In this first series of studies, we not only established the fact that multiturn injection is favorable for high intensity space-charge dominated beam, but also explored the efficiency of early capture by various voltage programs. The traditional method of adiabatic capture gives better efficiency and smoother beam distribution only for low intensity beams where space charge does not play a role during capture. However, for high intensity beams with strong space charge forces, slow voltage is not sufficient to contain the beam during early blow-up. We found the voltage wave form in Fig. 1 to be near the optimum for both early capture and later acceleration.

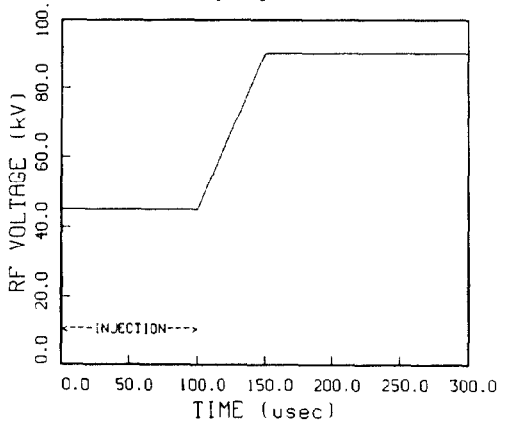

Fig. 1. RF Voltage program for cases 1-4.

Un-chopped beam

To further understand the beam behavior during multiturn injection, we did a second series of study and found that an rf capture of 90% can be achieved for the un-chopped beam, but for better capture efficiency, the Linac pulses would have to be chopped to eliminate those particles that have rf phase angles close to 0 and 2π. Indeed, chopping the Linac beam might become necessary because, due to the high beam current present in the Booster, even a small beam loss during the rf capture will result in high background radiation in and around the accelerator ring.

Chopped beam

We will present in greater detail the results of a third series of simulations of proton rf capture in the AGS Booster for the case of a chopped Linac beam. We studied 6 cases which we will label 1, 2, 3, 4.A, 4.B, and 4.C. All the cases were done for the voltage program shown in Fig. 1 and for an initial random uniform distribution in θ and gaussian distribution in E, with $\sigma_E \approx 0.2\ MeV$. We found that injecting at 45 kV and raising the voltage to 90 kV just after the end of injection was a good rf voltage scenario since it made the linear charge distribution somewhat smooth during injection time.The magnetic field used was given by

$$B(t) = B_i + (B_f - B_i)(\frac{t - t_i}{t_f - t_i})^{\alpha}, \quad (13)$$

where B_i =0.16 T (kinetic energy = 200 MeV) and B_f =0.54 T (kinetic energy = 1500 MeV) are the initial and final magnetic fields defined at times $t_i = 0$ and $t_f = 60\ ms$ (half the Booster cycle) respectively. The coefficient α was equal to 2 for case 1, 3/2 for case 2, 5/4 for case 3, and 1 for cases 4.A-4.C. The curves of the magnetic field programs are shown in Fig. 2.

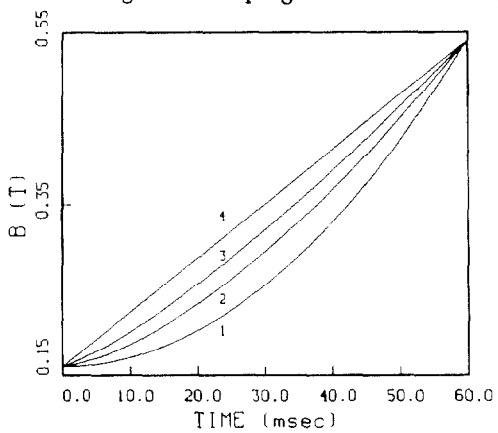

Fig. 2. Magnetic field curves for cases 1-4.

One first simulation was made for the case where we chopped 5° on each side of every bunch of the injected Linac beam (cases 1-4.A). This amounts to $\approx$ 8% of the total beam delivered by the source. The bucket areas and rf captures for theses cases are listed in Table 1.

Case #	α	500 μsec	1 ms
1	2	1.6/100	-
2	1.5	1.6/100	1.5/99
3	1.25	1.4/96	1.4/96
4.A	1	1.1/55	-
4.B	1	1.1/82	1.1/82
4.C	1	1.1/98	1.1/98

Table 1. List of bucket areas[$eV.sec$]/capture[%].

Notice that the rf captures for cases 1, 2 and 3 are all high but the rf capture for case 4.A is unacceptably small. This is due to the fact that $\dot{B}(t)$ starts from zero and increases more or less slowly therefrom for cases 1, 2 and 3 whereas it has a constant

value of $\approx 6.4\ T/s$ during the whole cycle for case 4.A. This makes the bucket area and the rf capture at injection for case 4.A much smaller than those of cases 1, 2 and 3. To illustrate this, we show the particle distribution in phase–space and the rf bucket at the beginning of injection for cases 1–3 and 4.A in Fig. 3.a and Fig. 3.b respectively. This demonstrates the fact that during capture, the rate of rise of the magnetic field should be kept as low as possible to be able to create the largest bucket area for the given initial voltage. With large $\dot{B}(t)$, as for case 4.A, the chopped beam loses its advantage since the bucket area is reduced to accommodate the large rate of acceleration required by the large $\dot{B}(t)$.

To improve the rf capture for case 4.A, we chopped more beam. We studied case 4.B, shown in Fig. 4, where we chopped $\approx 30°$ on one side of each bunch of the injected beam and $\approx 17°$ on the other. This corresponds to $\approx 50\%$ of the total beam from the source. This, of course, has improved the rf capture ($\approx 80\%$), but not enough to bring it to the level of cases 1–3.

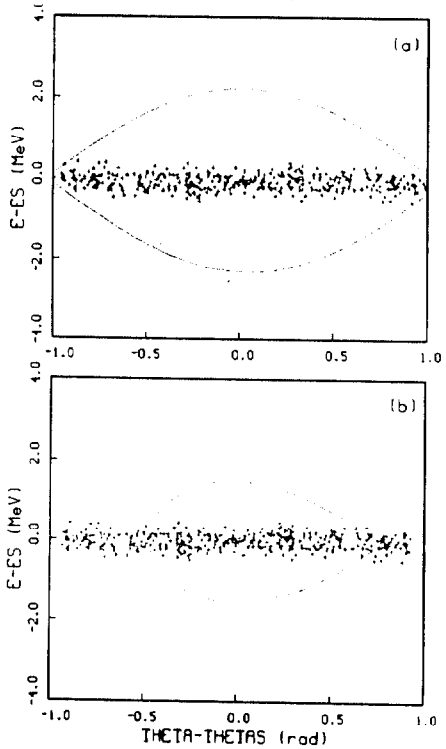

Fig. 3. a) Initial distribution and rf bucket for cases 1–3.
b) Case 4.A.

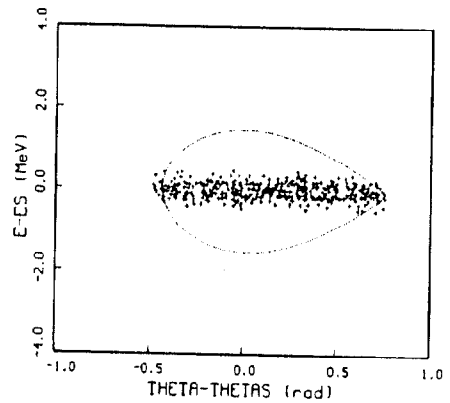

Fig. 4. Initial distribution and rf bucket for case 4.B.

The difference in this case can be accounted for by the bucket motion during the 100 μsec ($\approx$ 84 turns) injection time. This motion is related to the energy gain per turn of the synchronous particle which is given by

$$\Delta E/Turn[MeV] = 2\pi\rho R\dot{B}10^{-6}, \qquad (14)$$

where $\rho = 13.75\ m$ is the curvature radius of the Booster dipole magnets and $R = 32.114\ m$ is the average radius of the equilibrium orbit. With $\dot{B} \approx 6.4\ T/s$, we get $\Delta E/Turn \approx 17.7\ kV$. Therefore, the bucket moves up in energy by about 1.5 MeV during the 84 turns it takes to finish injection. We further modified the capture in case 4.C where the chopped Linac beam was injected at 201 MeV kinetic energy instead of 200 MeV. We show in Fig. 5 the evolution of the beam–rf bucket system during the first 100 μsec of the multiturn injection for case 4.C. This finally has made the rf capture at 500 μsec and 1 ms very close to that of cases 1–3 (see Table 1 and Fig. 6). However, the overall capture efficiency from the Linac drops from 92% to 50%, a price too high to be affordable.

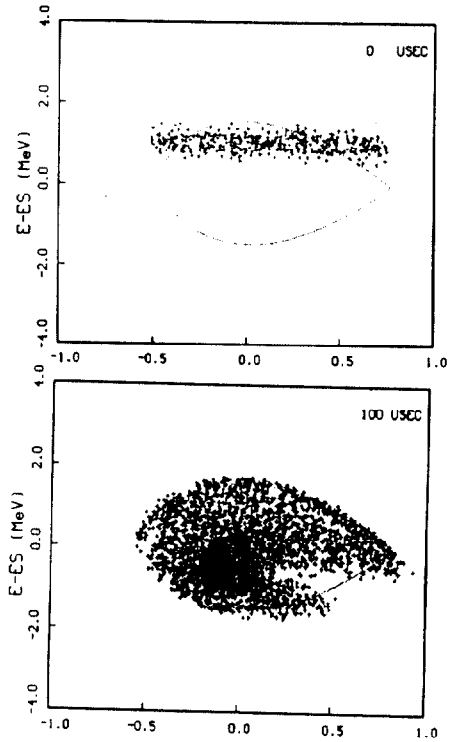

Fig. 5. Distribution for case 4.C at 0, 50, and 100 μsec.

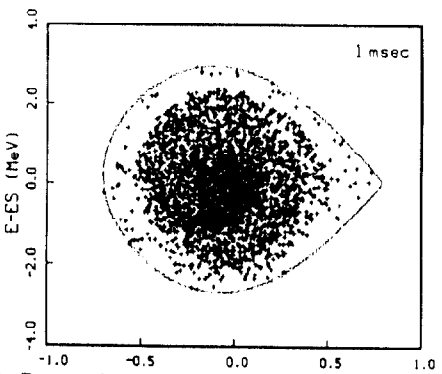

Fig. 6. Proton beam captured in the rf bucket at 1 $msec$. for case 4.C.

[1] Booster Design Manual, BNL, October 1986.
[2] J. A. MacLachlan, *Particle Tracking in E–ϕ Space as a Design Tool for Cyclic Accelerators*, Proceedings of The IEEE Particle Accelerator Conference, 1087 (1987).